

DIFFERENT TYPES OF ION POPULATIONS UPSTREAM OF THE 8 OCTOBER 2013
INTERPLANETARY SHOCK

PRIMOŽ KAJDIČ,¹ HELI HIETALA,² AND XÓCHITL BLANCO-CANO¹

¹*Instituto de Geofísica, Universidad Nacional Autónoma de México, Circuito de la investigación Científica s/n, Ciudad Universitaria, Delegación Coyoacán, C.P. 04510, Mexico City, Mexico*

²*Department of Earth, Planetary, and Space Sciences, University of California, Los Angeles, California, USA*

(Received July 1, 2016; Revised September 27, 2016; Accepted June 12, 2018)

Submitted to ApJL

ABSTRACT

We show for the first time that different types of suprathermal ion distributions may exist upstream of a single interplanetary shock. ACE and the two ARTEMIS satellites observed a shock on 8 October 2013. The ARTEMIS P1 and P2 spacecraft first observed field-aligned ions (P1) and gyrating ions (P2) arriving from the shock. These were followed by intermediate ions and later by a diffuse population. At the location of the P2 the shock exhibited an Alfvénic Mach number of $M_A=5.7$ and was marginally quasi-perpendicular, ($\theta_{Bn}=47^\circ$). At P1 spacecraft the shock was weaker ($M_A=4.9$) and more perpendicular ($\theta_{Bn}=61^\circ$). Consequently the observed suprathermal ion and ultra low frequency wave properties were somewhat different. At P2 the ULF waves are more intense and extend farther upstream from the shock. The energies of field aligned and gyrating ions in the shock rest frame were ~ 20 keV, which is much more than in the case of the stronger ($M_A=6-7$) Earth's bow-shock, where they are less than 10 keV.

Keywords: solar wind — interplanetary medium — shock waves — acceleration of particles — waves

1. INTRODUCTION

High energy particles, such as Solar Energetic Particles (SEP; e.g., Schwenn 2006; Reames et al. 1996) and Energetic Storm Particles (ESP; e.g., Cohen 2006), are common in the Solar System. It is important to study them since they present hazard for spacecraft, humans in space and even our ground based technologies such as power grids. The SEPs are also interesting since they can be used to study elemental and isotopic composition of the Sun and particle acceleration mechanisms (Williams et al. 1998).

Significant accelerators of energetic particles in the Solar System are collisionless shocks which belong to two major groups: planetary and interplanetary (IP) shocks. Planetary shocks form when the solar wind (SW) encounters obstacles such as planets with intrinsic magnetospheres (e.g., Mercury, Earth, Saturn, Jupiter; see for example, Bagenal 1992; Russell 1993), planets with induced magnetospheres such as Venus and Mars (e.g., Luhmann et al. 2004) and active comets (e.g., Cravens and Gombosi 2004). Due to their form, planetary shocks are also called bow-shocks. The major drivers of the IP shocks are interplanetary coronal mass ejections (ICME; Sheeley et al. 1985) and stream interaction regions (SIR; Gosling and Pizzo 1999). Especially the ICME driven IP shocks have been recognized as important accelerators of energetic particles (e.g., Kahler 2003; Manchester et al. 2005).

When the fast magnetosonic Mach number M_{ms} of a collisionless shock exceeds a certain critical value M_c , the shock is called supercritical. The M_c depends on several parameters, such as the angle between the direction of the upstream interplanetary magnetic field (IMF) and the shock normal, θ_{Bn} (Edminston and Kennel 1986). The supercritical shocks dissipate the kinetic energy of the incoming SW by energizing and reflecting a portion of the incident particles (ions, electrons) back upstream. Shocks are further divided according to θ_{Bn} . For $\theta_{Bn} < 45^\circ$ ($\geq 45^\circ$), they are called quasi-parallel (quasi-perpendicular). In the case of the Earth's bow-shock the reflected ions have been observed for $\theta_{Bn} \leq 70^\circ$ (e.g., Eastwood et al. 2005). These are also called backstreaming particles. Interaction of backstreaming ions with the incident SW ions results in the growth of ultra-low frequency (ULF) waves (e.g., Dorfman et al. 2017). At Earth these waves have periods of ~ 30 s on average. The

region upstream of quasi-parallel shocks populated with ULF waves (suprathermal ions) is called the ULF wave (suprathermal ion) foreshock (e.g., [Eastwood et al. 2005](#), and references therein).

In the case of Earth there are plenty of observations of backstreaming particles. Near the leading edge of its foreshock a spacecraft first observes *field-aligned ion beams* (FAB; [Gosling et al. 1978, 1979](#); [Thomsen 1985](#); [Kis et al. 2007](#); [Meziane et al. 2013](#)). These ions stream upstream along the IMF and exhibit highly collimated, beam-like distributions in velocity space. Their energies are below 10 keV and they are not accompanied by ULF waves although they are responsible for their generation ([Thomsen 1985](#); [Eastwood et al. 2005](#)). The FABs are also considered to be the seeds of the so called *diffuse ions* (e.g., [Fuselier et al. 1986](#); [Kis et al. 2004](#)), which show almost isotropic distributions in the SW frame with a small average bulk velocity directed sunward. These ions are observed upstream of the almost parallel section of the Earth's bow-shock, they exhibit energies up to several hundreds of keV, and are accompanied by compressive ULF fluctuations. The third kind of suprathermal ions is called *intermediate* ([Paschmann et al. 1979](#)) with distributions intermediate between the FABs and diffuse ions. They are thought to form because farther from the edge of the foreshock the ULF waves disrupt the FAB ions, scattering them in pitch angle (PA) which leads to crescent-shaped and later to diffuse distributions. Other ion distributions have also been observed: [Paschmann et al. \(1982\)](#) observed the so called *gyrating ions* that exhibit distribution peaks at non zero PAs relative to the IMF. Special cases of gyrating distributions are *gyrotropic ions* with distribution being a torus with a symmetry axis parallel to the IMF direction ([Winske et al. 1984](#)) and *gyrophase-bunched ions* ([Gurgiolo et al. 1981, 1983](#); [Eastman et al. 1981](#); [Thomsen 1985](#)).

In order to distinguish between the FABs and the gyrating ions we use criteria similar to [Savoini et al. \(2013\)](#) and references therein. Backstreaming ions are classified as FABs if they exhibit pitch angles between $\sim 0^\circ$ and $\sim 30^\circ$, while they are denominated as gyrating ions if their pitch angles extend to larger values (e.g., $\sim 90^\circ$).

Although ions in suprathermal particle energy range have been observed upstream of IP shocks at 1 A.U., they mostly exhibit diffuse distributions (e.g., [Armstrong et al. 1970](#); [Bavassano-Cattaneo et al.](#)

1986; Gosling 1983; Gosling et al. 1984). It is not clear whether these ions were actually accelerated by IP shocks near 1 AU or whether they are just low-energy parts of SEPs.

Only two works report observations of ion populations other than diffuse upstream of IP shocks: Viñas et al. (1984) show ion spectra upstream of an IP shock observed on 3 February 1978 obtained by the Voyager 1 Faraday cups, however no distributions were obtained. Tokar et al. (2000) reported observations of suprathermal FABs upstream of an IP shock observed by the ACE mission (Stone et al. 1998) on 7 April 1998, but the authors could not determine details of the ion distribution functions.

Gosling (1983) stated that we should not expect to observe non-diffuse ion distributions upstream of IP shocks. The IP shocks have large curvature radii (of the order of 0.5 AU at heliocentric distance of 1 A.U. compared to a few tens of Earth radii, R_E , of the Earth's bow-shock) which means that the magnetic field lines stay connected to them for very long times, typically for a day or longer. At planetary shocks these times are of the order of ten minutes. In the case of the planetary shocks we can observe the process of particle acceleration from the beginning, when B-field lines first connect to the bow-shock. In the case of IP shocks we expect to observe acceleration processes at later stages, hence we would detect diffuse ions. Another problem is that spacecraft are usually not equipped to measure ion distributions continuously from SW thermal to suprathermal energies.

Here we present the first observations of different types of suprathermal ion distributions upstream of a single IP shock that was observed on 8 October 2013, by ACE and the ARTEMIS P1 and P2 spacecraft. We combine the cross-calibrated measurements of the ARTEMIS thermal and energetic particle sensors, obtaining 3D ion distributions covering the key suprathermal energy range. The P1 and P2 spacecraft first observed field-aligned and gyrating ions arriving from the IP shock. As the shock approached, the ion distributions changed to intermediate and then to almost diffuse. These observations confirm that the same ion acceleration mechanisms that are at work at Earth's bow-shock also act at IP shocks. However, in the case of the latter the ions can be accelerated to higher energies compared to those at Earth's bow-shock.

2. DATASETS

We use measurements of the two identical ARTEMIS spacecraft orbiting the Moon ([Angelopoulos 2010](#)). Magnetic field measurements are provided by the Fluxgate Magnetometer (FGM, [Auster et al. 2008](#)). The FGM data are only available in spin (4 s) cadence. Plasma measurements are provided by the Electrostatic Analyzer (ESA, [McFadden et al. 2008](#)) and Solid State Telescope (SST, [Angelopoulos 2008b](#)). ESA provides ion measurements between ~ 5 eV and ~ 25 keV. SST provides ion data between 25 keV and 6 MeV.

During the time of interest ESA and SST switched from the Fast Survey Mode to the Slow Survey Mode which affects the cadence of the omni-directional ion spectra and of three-dimensional ion distributions. A detailed description of the ESA and SST operational modes and the explanation on how the combined spectra and distributions from both instrument were obtained, are available in the appendix.

We also use the ACE magnetic field data from the MAG instrument ([Smith et al. 1998](#)) with 1 second cadence.

All the spacecraft coordinates and measured vectors are given in Geocentric Solar Ecliptic (GSE) coordinate system which is defined so that the X-axis points from the Earth towards the Sun and the Z-axis towards the ecliptic North pole. The Y axis completes the right-hand system.

3. OBSERVATIONS

We selected the 8 October 2013 IP shock from the *Catalog of IP shocks observed in the Earth's neighbourhood by multiple spacecraft between 2011-2014* available at <http://usuarios.geofisica.unam.mx/primoz/IPShocks.html>. ACE observed the shock at 19:40:49 UT while the ARTEMIS P1 and P2 spacecraft observed it at 20:16:56 UT and 20:16:24 UT, respectively. At the times of the shock passage the three spacecraft were located at: $(247.0, -25.0, 0.9) R_E$, $(56.5, 20.6, -4.6) R_E$ and $(56.2, 25.7, -4.6) R_E$ (Figure 1).

The separations of the ARTEMIS spacecraft from the Moon were 10.2 and 2.6 lunar radii (R_L) along the Sun-Moon line and 2.0 R_L and 10.7 R_L perpendicular to it for P1 and P2, respectively. According to [Harada et al. \(2015\)](#) these distances are large enough so that no significant Moon-related ion fluxes

should be detected by either of the ARTEMIS spacecraft. Also, the IMF orientation indicates that the spacecraft were not magnetically connected to the Moon nor to the Earth's bow-shock (Figure 1).

The shock normal and the θ_{Bn} at each spacecraft were calculated using the magnetic coplanarity method (e.g., [Schwartz 1998](#)): (-0.02, 0.96, -0.27) and 74° at ACE, (-0.81, 0.1, 0.58) and 61° at P1 and (-0.8, 0.13, 0.59) and 47° at P2 (other methods, such as mixed methods ([Schwartz 1998](#)) provided very similar results). The θ_{Bn} values at P1 and P2 do not overlap regardless of the method used. The estimated shock speeds in the spacecraft frame and the Alfvénic Mach numbers M_A , were calculated to be 428 kms^{-1} and 4.9 at P1 and 456 kms^{-1} and 5.7 at P2. The θ_{Bn} was smaller at P2, where the M_A was higher. While the shock normal directions are similar at P1 and P2, at ACE the normal differs by 90° . This is not surprising since it was shown by [Szabo \(2005\)](#) that the IP shock normals may differ greatly when the spacecraft separations perpendicular to the Sun-Earth line are of several tens of R_E .

3.1. *Reflected ions*

The 8 October 2013 shock was driven by a complex event composed of a SIR and at least one ICME. Figure 2 shows ARTEMIS P1 (panels a - c) and P2 (panels d - f) observations from 19:10 UT to 20:30 UT. The panels a) and d) exhibit combined SST and ESA ion spectra (the colors represent the logarithm of the particle energy flux), panels b) and e) exhibit IMF components and c) and f) panels show the SW velocity components. The red vertical lines and roman numerals show times of the distributions exhibited in Figure 3.

Figure 3 shows particle (ion) distribution functions (PDF) at five different times obtained by P1 (panels i - v) and P2 (panels vi - x) spacecraft. In both cases there are four PDFs observed upstream and one downstream of the shock. Note that the ion spectra in Figure 2 and PDFs in Figure 3 were made with different datasets resulting in some discrepancies between the two figures (see appendix).

On panels a) and d) of Figure 2 we can see a red trace centered at $\sim 470 \text{ eV}$, which is the SW. It corresponds to the red circular spot on all panels in Figure 3. The FABs are barely detected by ESA, but they appear as a light-blue trace at $\lesssim 200 \text{ keV}$ in the SST part of the spectra.

In all panels of Figure 3, part of the ion PDF around the SW core is missing. This occurs when the intensity of suprathermal ions is less than the sensitivity of the instrument. Figure 5 in the appendix illustrates this by showing the signal from both instruments and their corresponding one-count levels. For ESA, the intensity of the reflected suprathermal ions was mostly below the one-count level, except during the last ~ 15 minutes before the shock crossing. In contrast, the lowest energy channels of SST are much more sensitive and can detect these suprathermal ions.

We first look at the P1 distributions and ion spectra. Figure 3i) shows the first particle distribution function featuring FABs during the time interval centered at 19:15:06 UT. The FABs appear as a blue and purple trace with velocities at $V_B \sim 2000 \text{ km s}^{-1}$ and V_V between -600 km s^{-1} and 100 km s^{-1} . These velocities correspond to energies of $\sim 21 \text{ keV}$ in the spacecraft frame. We also calculate suprathermal ion kinetic energies in the shock rest frame by subtracting the shock velocity with respect to the spacecraft (428 km s^{-1} along the shock normal) but the result remains roughly the same. Such kinetic energies of the FABs are much higher than in the case of the Earth's bow-shock, where the FABs exhibit energies less than 10 keV (Thomsen 1985). It seems that although the IP shock studied here had a lower M_A than the typical Earth's bow-shock near its subsolar point, the IP shock is able to accelerate the FABs to much higher energies. This is probably related to IP shock's large curvature radii and long connection times of the IMF field lines to the shock. Ions that reflect at quasi-perpendicular section of the IP shock remain at such section for longer periods and consequently the shock drift and shock surfing acceleration mechanisms act for longer periods accelerating ions to higher energies.

The flux of the reflected ions in Figure 2a) intensifies with time and their maximum energy increases and eventually reaches $\sim 200 \text{ keV}$. Figure 3ii) shows the PDF at 19:21:55 UT. We can see that the ion beam has broadened. The peak of the distribution lies along the magnetic field but the beam extends to the upper right quadrant. The maximum velocities of the ions are $\sim 6000 \text{ km s}^{-1}$ in the spacecraft frame, corresponding to energies of $\sim 190 \text{ keV}$. Just before the shock (panel iv) the ion PDF becomes diffuse, as revealed by the SST measurements. Downstream of the shock (panel v) the ions are heated and their distributions become isotropic.

In the case of the P2 spacecraft the observed PDFs look a bit different. First, we note an intense spot in lower-right quadrant on panels vi)-viii) marked by a crossed purple ellipse. A careful inspection of the PDFs in the X_{GSE} - Y_{GSE} plane revealed that this signal comes from the direction of the Moon. It is not related to any ions but it is caused by the reflected photons coming from the Moon, so we will disregard it. We still see ions in the upper right quadrant on panel vi). These are non-gyrotropic ions. At later times (panels vii and viii) we observe intermediate ion PDFs and just before the shock arrival (panel ix) the ion PDF is almost completely diffuse. Again, downstream of the shock we observe an isotropic, heated ion PDFs (panel x).

3.2. *Upstream waves*

Figure 4 shows B magnitude (black) and $-B_{x,GSE}$ component (blue) on panels i) and iv) (corresponding to P1 and P2 observations, respectively). Panels ii) and v) show wavelet spectra of B magnitude while panels iii) and vi) show the spectra for the $B_{x,GSE}$ component. The shaded intervals correspond to times when the upstream ULF waves are present. The waves appear ~ 7.8 minutes before the shock arrival in the case of P2 and ~ 5.2 minutes before in the case of P1. At first they are highly transverse, but they become more compressive closer to the shock front. Their frequencies are between 0.02 Hz and 0.1 Hz (periods between 10 s and 50 s). By comparing Figures 2 and 4 we can see that the FABs coincide with times when no ULF waves are present, but that the almost diffuse ion PDFs appear together with upstream ULF waves that exhibit an important compressive component.

4. DISCUSSION AND CONCLUSIONS

We report the first observations of different suprathermal ion distributions upstream of the single 8 October 2013 IP shock. These observations were made with the two ARTEMIS spacecraft. The shock properties, the ion PDFs and the upstream ULF wave foreshocks differ at the two observational points. The shock is weaker and quasi-perpendicular ($M_A=4.9$, $\theta_{Bn}=61^\circ$) at P1, while it is stronger and less quasi-perpendicular ($M_A=5.7$, $\theta_{Bn}=47^\circ$) at P2. Consequently, at P2 the ULF waves appear before than at P1 and they are more intense.

Ion distributions vary from FABs (at P1) and gyrating ions (at P2) upstream of the shock, to intermediate and finally to diffuse distributions just before the shock arrival. The FABs and the gyrating ions are observed in the absence of any ULF fluctuations, while the diffuse ions coincide with partially compressive ULF waves.

The energies of the FABs in the shock rest frame are of the order of 20 keV, which is much more than in the case of the Earth's bow-shock, where they are $\lesssim 10$ keV. This is probably a consequence of larger curvature radii of IP shocks and longer connection times of IMF lines to the IP shock surface. Under these conditions ions travel larger distances with $\theta_{Bn} < 60^\circ$ meaning that the shock drift and shock surfing mechanisms (Hudson and Kahn 1965; Lever et al. 2001) accelerate them to higher energies.

In addition to the curvature radius and M_A , there are other factors that influence the efficiency of ion acceleration at shocks, such as background turbulence and plasma beta. One should also keep in mind that the quasi-perpendicular, supercritical shocks undergo continuous self-reformation and this shock nonstationarity additionally impacts the ion reflection and energization (e.g., Mazelle et al. 2010; Lobzin et al. 2007; Yang et al. 2009).

The energies of the observed diffuse ions are $\lesssim 200$ keV, which is similar to ions near the Earth's bow-shock.

This work has been supported by the International Space Science Institute (ISSI). PK's and XBC's work was supported by DGAPA/PAPIIT grants IA104416 and IN105014 and by CONACYT grant 179588. HH's work was supported by NASA contract NAS5-02099.

REFERENCES

- | | |
|--|---|
| <p>Angelopoulos, V., Sibeck, D. G., Farrell, W. M. et al. 2008, NLSI Lunar Science Conference, July 20-23, LPI Contribution No. 1415, abstract no. 2161.</p> | <p>Angelopoulos, V., Sibeck, D. G., Carlson, C. W. et al. 2008, <i>SSRv</i>, 141, 453, doi:10.1007/s11214-008-9378-4.</p> <p>Angelopoulos, V. 2010, <i>SSRv</i>, 165, 3, doi:10.1007/s11214-010-9687-2.</p> |
|--|---|

- Auster, H. U., Glassmeier, K. H., Magnes, W. et al. 2008, *SSRv*, 141, 235, doi:10.1007/s11214-008-9365-9.
- Armstrong, T. P., Krimigis, S. M., Behannon K. W. 1970, *J. Geophys. Res.*, 75(31), 5980, doi:10.1029/JA075i031p05980.
- Bagenal F. 1992, *Annu. Rev. Earth Planet Sci.*, 20, 289
- Bavassano-Cattaneo, M. B., Tsurutani, B. T., Smith, E. J., Lin, R. P. 1986, *J. Geophys. Res.*, 91(A11), 11929, doi:10.1029/JA091iA11p11929.
- Cohen, C. M. S. 2006, in *Solar Eruptions and Energetic Particles*, Vol. 165 ed. N. Gopalswamy, R. Mewaldt, & J. Torts, (Washington, D.C.: AGU), 275
- Cravens, T. E, Gombosi, T. I. 2004, *AdSpR*, 33, 196, doi:10.1016/j.asr.2003.07.053.
- Dorfman, S., Hietala, H., Astfalk, P. and Angelopoulos, V. 2017, *Geophys. Res. Lett.*, 44, 2120, doi:10.1002/2017GL072692.
- Eastman, T. E. Anderson, R. R., Frank, L. A., Parks, G. K. 1982, *J. Geophys. Res.*, 86, 4379.
- Eastwood, J.P., Lucek, E.A., Mazelle, C. et al. 2005, *SSRv*, 118, 41, doi:10.1007/s11214-005-3824-3
- Edmiston, J. P., Kennel, C. P. 1986, *J. Geophys. Res.*, 91(A2), 1361 doi:10.1029/JA091iA02p01361.
- Fuselier, S. A., Thomsen, M. F., Gosling, J. T., Bame, S. J. 1986, *J. Geophys. Res.*, 91, 91.
- Gosling, J. T., Asbridge, J. R., Bame, S. J., Paschmann, G., Sckopke, N. 1978, *Geophys. Res. Lett.*, 5, 957, doi:10.1029/GL005i011p00957.
- Gosling, J. T., Asbridge, J. R., Bame, S. J., Paschmann, G., Sckopke, N. 1978, *Geophys. Res. Lett.*, 5,957.
- Gosling, J. T. 1983, *SSRv*, 34, 113, doi:10.1007/BF00194621.
- Gosling, J. T., Bame, S. J., Feldman, W. C., Paschmann, G., Sckopke, N., Russell, C. T. 1984, *J. Geophys. Res.*, 89(A7), 5409, doi:10.1029/JA089iA07p05409.
- Gosling, J. T., Robson, A. E. 1985, *Ion Reflection, Gyration, and Dissipation at Supercritical Shocks*, in *Collisionless Shocks in the Heliosphere: Reviews of Current Research* (eds B. T. Tsurutani and R. G. Stone), American Geophysical Union, Washington, D. C.. doi: 10.1029/GM035p0141
- Gosling, J. T., Pizzo, V. J. 1999, *SSRv*, 89, 21, doi:10.1023/A:1005291711900.
- Gurgiolo, C., Parks, G. K., Mauk, B. H., Lin, C. S., Anderson, K. A., Lin, R. P., Reme, H. 1981, *J. Geophys. Res.*, 86, 4415.
- Gurgiolo, C., Parks, G. K., Mauk, B. H. 1983, *J. Geophys. Res.*, 88, 9093.
- Harada, Y., Halekas, J. S., Poppe, A. R., Tsugawa, Y., Kurita, S., McFadden, J. P. 2015, *J. Geophys. Res.*, 120, 4907, doi:10.1002/2015JA021211.

- Hietala, H., Drake, J. F., Phan, T. D., Eastwood, J. P. and McFadden, J. P. 2015 *Geophys. Res. Lett.*, 42, 7239, doi:10.1002/2015GL065168.
- Hietala, H., Artemyev, A. V. and Angelopoulos, V. 2017, *J. Geophys. Res.*, 122, 2010, doi:10.1002/2015JA021166.
- Hudson, P. D. and Kahn, F. D. 1965, *MNRAS*, 131, 23-49.
- S.W. Kahler, S. W. 2003, *AdSpR*, 32, 2587, doi:10.1016/j.asr.2003.02.006.
- Kis, A., Scholer, M., Klecker, B., Möbius, E., Lucek, E. A., Rème, H., Bosqued, J. M., Kistler, L. M. and Kucharek, H. 2004, *Geophys. Res. Lett.*, 31, L20801, doi:10.1029/2004GL020759.
- Kis, A., Scholer, M., Klecker, B., Kucharek, H., Lucek, E. A., and Rème, H. 2007, *AnGeo*, 25, 785, doi:10.5194/angeo-25-785-2007.
- Lever, E. L., Quest, K. B., Shapiro, V. D. 2001, *Geophys. Res. Lett.*, 28: 1367m, doi:10.1029/2000GL012516.
- Lobzin, V. V., Krasnoselskikh, V. V., Bosqued, J.-M., et al. 2007, *Geophys. Res. Lett.*, 34, L05107
- Luhmann, J. G., Ledvina, S. A., Russell, C. T. 2004, *AdSpR*, 33, 1905, ISSN 0273-1177, doi:10.1016/j.asr.2003.03.031.
- Manchester W. B. IV, Gombosi T. I., Zeeuw D. L. et al. 2005, *ApJ*, 622, 1225
- Mazelle, C., Lembege, B., Morgenthaler, A., et al. 2010, in *AIP Conf. Proc.* 1216, 12th International Solar Wind Conference (Melville, NY: AIP), 471
- McFadden, J. P., Carlson, C. W., Larson, D. et al. 2008, *SSRv*, 141, 277. doi:10.1007/s11214-008-9440-2.
- Meziane, K., Hamza, A. M., Wilber, M., Mazelle, C. and Lee, M. A. 2013, *J. Geophys. Res.*, 118, 6946, doi:10.1002/2013JA019060.
- Narita, Y., Glassmeier, K.-H., Schafer, S., et al. 2004, *AnGeo*, 22, 2315, doi:10.5194/angeo-22-2315-2004.
- Paschmann, G., Sckopke, N., Bame, S. J., Gosling, J. T., Russell, C. T., Greenstadt, E. W. 1979, *Geophys. Res. Lett.*, 6,209.
- Paschmann, G., Sckopke, N., Bame, S. J., Gosling, J. T. 1982, *Geophys. Res. Lett.*, 9, 881.
- Reames, D. V., Barbier, L. M., Ng, C. K. 1996, *ApJ*, 466, 473, doi:10.1086/177525.
- Runov, A., Angelopoulos, V., Gabrielse, C., Liu, J., Turner, D. L. and Zhou, X.-Z. 2015, *J. Geophys. Res.*, 120, 4369, doi: 10.1002/2015JA021166.
- Russell, C. T. 1993, *J. Geophys. Res.*, , 98(E10), 18681, doi:10.1029/93JE00981.
- Savoini, P., Lembege, B., Stienlet, J. 2013, *J. Geophys. Res.*, 118, 1132, doi:10.1002/jgra.50158.
- Schwartz, S. J. 1998, in *ESA/ISSI 1*, 249
- Schwenn, R. 2006, *LRSP*, 3, 2

- Sheeley Jr., N. R., R. A. Howard, M. J. Koomen, D. J. Michels, R. Schwenn, K. H. Mhlhuser, Rosenbauer, H. 1985, *J. Geophys. Res.*, 90(A1), 163, doi:10.1029/JA090iA01p00163.
- Smith, C. W., Acuña, M. H., Burlaga, L. F., L'Heureux, J., Ness, N. F., Scheifele, J. 1997, 86, 613, doi:10.1023/A:1005092216668.
- Stone, E. C., Frandsen, A. M., Mewaldt, R. A., Christian, E. R., Margolies, D., Ormes, J. F., Snow, F. 1998, *SSRv*, 86, 1, doi:10.1023/A:1005082526237.
- Szabo, A. 2005, *AIP Conference Proceedings* 781, 37, doi: <http://dx.doi.org/10.1063/1.2032672>.
- Thomsen, M. F. 1985,. *Upstream Suprathermal Ions, in Collisionless Shocks in the Heliosphere: Reviews of Current Research* (eds B. T. Tsurutani and R. G. Stone), American Geophysical Union, Washington, D. C.. doi: 10.1029/GM035p0253
- Tokar, R. L., Gary, S. P., Gosling, J. T., McComas, D. J., Skoug, R. M., Smith, C. W., Ness, N. F., Haggerty, D. 2000, *J. Geophys. Res.*, 105, 7521
- Viñas, A. F., Goldstein, M. L., Acuña, M. H. 1984, *J. Geophys. Res.*, 89, 3762
- Williams, D., Leske, R., Mewaldt, R. et al. 1998, *SSRv*, 85, 379, doi:10.1023/A:1005143710585.
- Winske, D., Wu, C. S., Li, Y. Y., Zhou G. S. 1984 *J. Geophys. Res.*, 89, 7327.
- Yang, Z. W., Lu, Q. M., Lembege, B., Wang, S. 2009, *J. Geophys. Res.*, 114, A03111

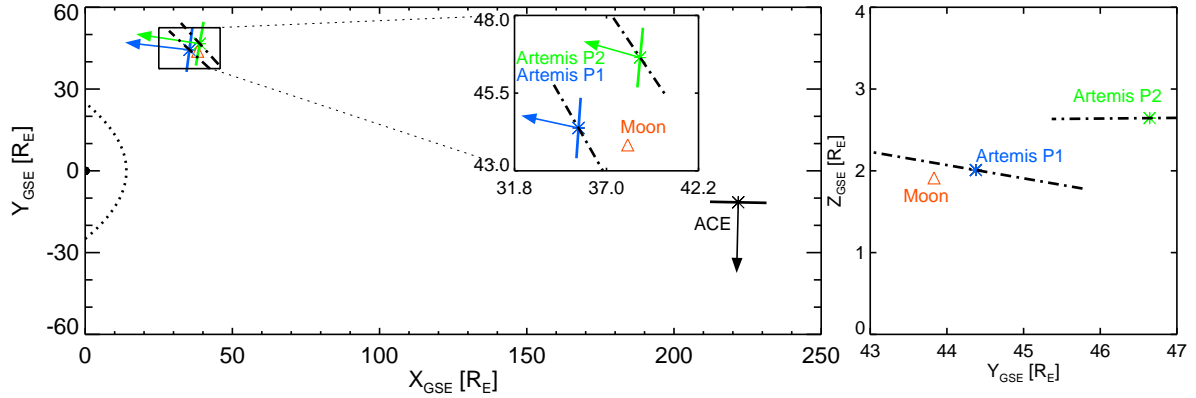


Figure 1. Positions of both ARTEMIS spacecraft, the ACE spacecraft and the Moon in GSE XY plane on 8 October 2013 at times of the shock detection. Positions of P1 and P2 spacecraft are marked with blue and green asterisks, respectively. The red triangle marks the position of the Moon. The arrows show the projections of shock normals at each spacecraft. In the case of P1 and P2 the black dash-dotted lines represent the orientation of the IMF. The small black dot at the origin represents the Earth while the black dotted curve surrounding it represents its nominal bow-shock (we use the model bow-shock from [Narita et al. \(2004\)](#)).

APPENDIX

A. CONTENTS

This section contains information on how the combined ion omni directional spectra and three dimensional particle distribution functions were obtained from the data from the ESA and SST instruments and an explanation on their operational modes. We also show the sensitivities (one count levels) of both instruments and compare them with the observations.

B. ESA AND SST OPERATIONAL MODES

The ARTEMIS ESA and SST instruments were in magnetospheric Fast Survey Mode until $\sim 19:29$ UT. After that they were in magnetospheric Slow Survey Mode. While each ESA and SST sample is always collected over one spacecraft spin period (~ 4 seconds), during the two modes, there are differences in the angular, energy, and temporal resolutions of various downlinked data products.

During Fast Survey, we have three-dimensional ESA “full mode” ion distributions (88 angles, 32 energies) available every 32 spins (~ 2.1 minutes) and “reduced mode” ion distributions (50 angles,

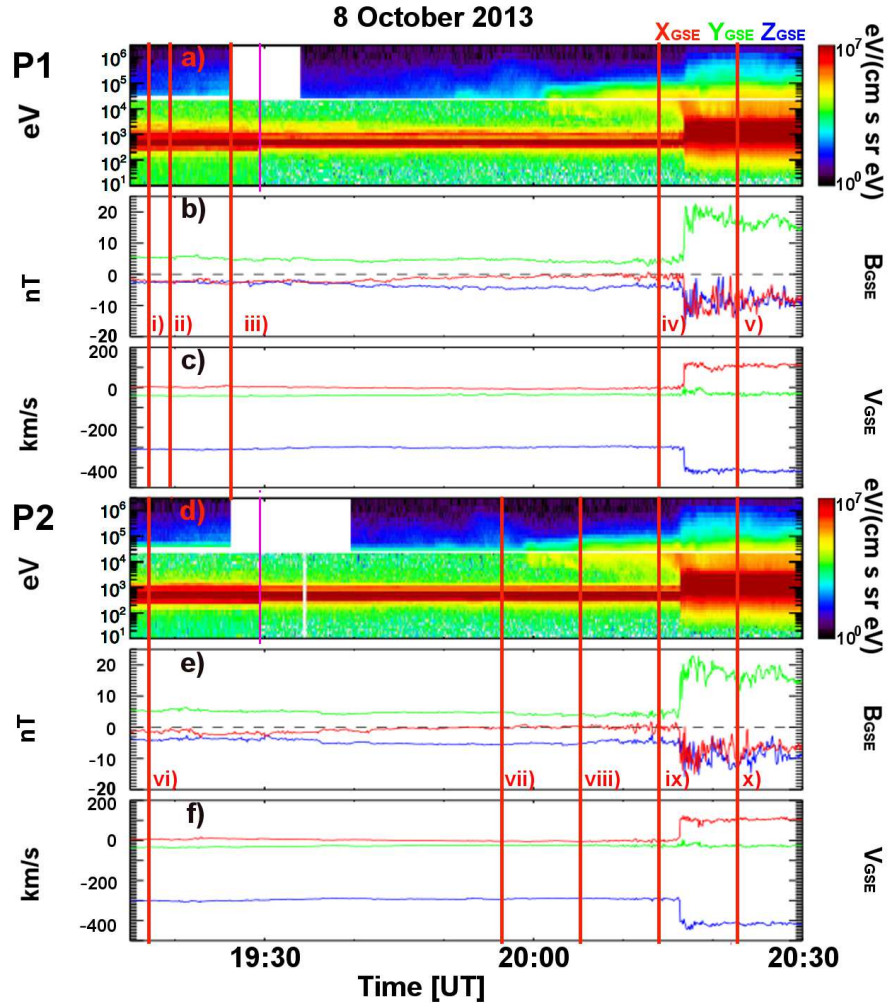


Figure 2. ARTEMIS P1 and P2 observations. a) and d): dynamic ion spectra from SST and ESA. b) and e): interplanetary magnetic field components. c) and f): SW velocity components. The red, green and blue curves on IMF and velocity panels represent the X_{GSE} , Y_{GSE} and Z_{GSE} components, respectively. Roman numbers and vertical red lines mark the times of ion distributions shown in Figure 3. Vertical purple lines mark the times when the ion instruments switched the operational modes.

24 energies) available for every spin. SST “full mode” ion distributions (64 angles, 16 energies) are also available for every spin.

During Slow Survey mode, ESA “full mode” ion distributions are available every 128 spins (~ 9 minutes), and “reduced/omni-directional” distributions (1 angle, 32 energies) are available every spin. SST “full mode” ion distributions are available every 64 spins (~ 4.3 minutes) and “reduced/omni-directional” distributions (1 angle, 16 energies) are available for every spin.

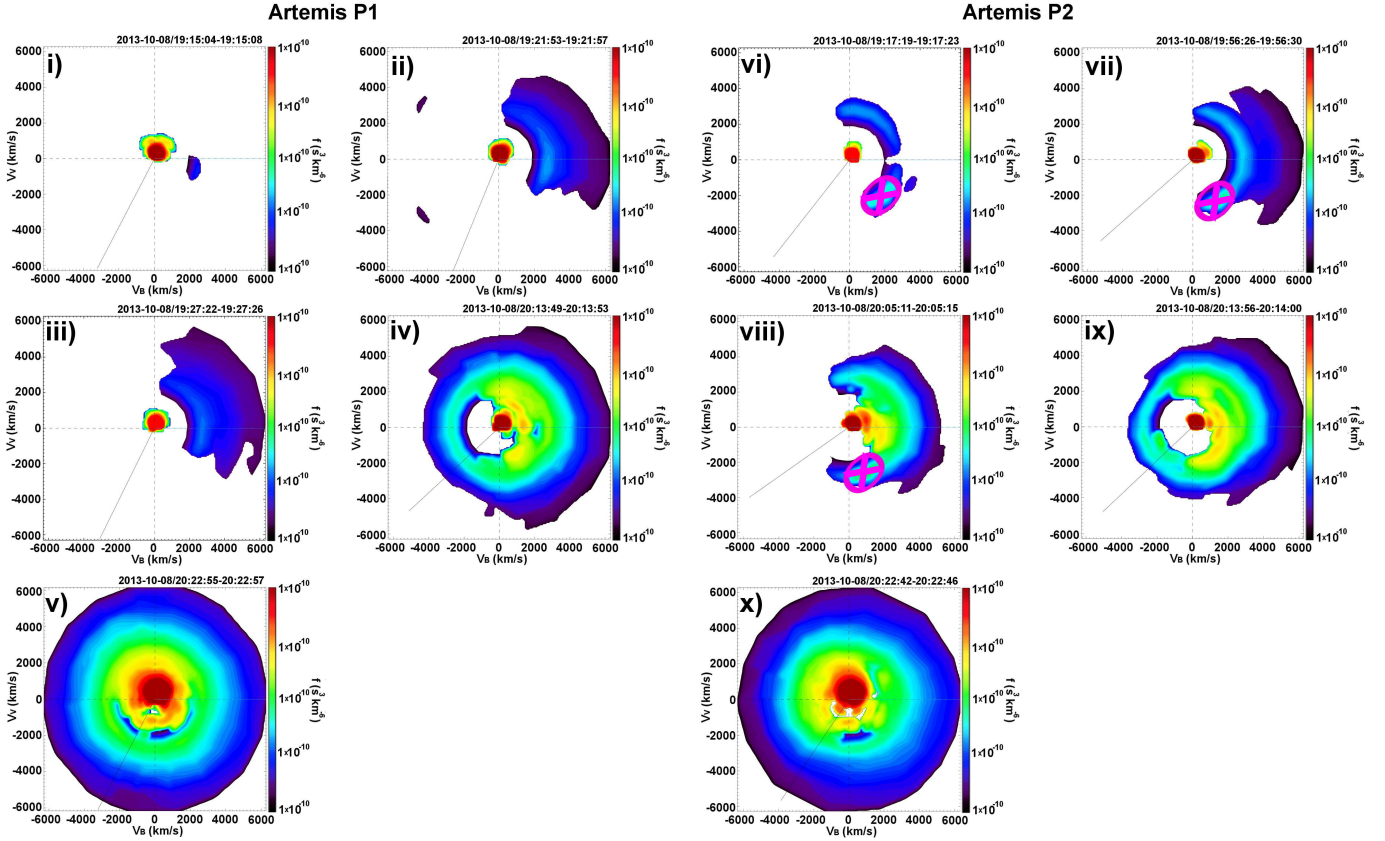


Figure 3. Ion distribution functions measured by ARTEMIS P1 (i-v) and P2 (vi-x) spacecraft at five different times. The distribution slice planes are defined so that they contain the IMF and the SW velocity vectors. The x-axis (V_B) points along the IMF and the y-axis (V_V) points along the SW velocity component perpendicular to the IMF. The black lines show the Sun direction. Colors represent the logarithm of the particle phase space density. Crossed purple ellipses in panels vi), vii) and viii) mark the signal due to photons reflected from the lunar surface.

The mode change may sometimes result in a minor data loss of some products. Note also that some ground calibrations are only possible for the higher angular resolution data products.

C. COMBINED OMNI-DIRECTIONAL ION SPECTRA AND THREE-DIMENSIONAL ION DISTRIBUTIONS

The high time-resolution omni-directional ion spectra shown in Figure 2 of this study were constructed in the following way. During the early part of the interval, when the spacecraft were in Fast Survey mode, we have plotted the spectra of ESA reduced mode distributions and SST full mode distributions in the same panel (no interpolation, as evidenced by the small white horizontal gap).

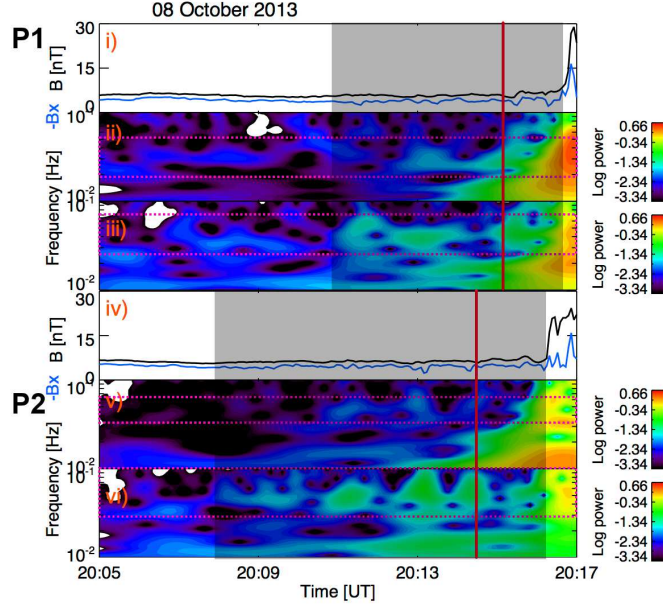


Figure 4. i) and iv): IMF magnitude (black) and $-B_x$ component (blue) from ARTEMIS P1 and P2 spacecraft, respectively. ii) and v): Wavelet spectra of the IMF magnitude. iii) and vi): Wavelet spectra of the B_x component. Horizontal purple lines delimit the frequency range of interest. Vertical red lines show times of diffuse ions from Figure 3. The intervals of upstream ULF waves are shaded in gray.

During the later part of the interval, when the spacecraft were in Slow Survey mode, we have plotted the ESA and SST reduced/omni-directional distributions in the same panel (no interpolation). There were minor losses of the reduced/omni-directional data products during the mode change, which manifest as the white gaps in Figure 2 panels a and d.

To make the ion distribution slices shown in Figure 3, we have combined the ESA and SST full mode (highest energy and angular resolution) measurements using 3D interpolation. (Note that the cadence at which these measurements are available depends on which Survey mode the instruments were in, as described above.) This type of combined distributions have recently been used in several ARTEMIS/THEMIS studies of different plasma regions (see e.g. [Dorfman et al. 2017](#); [Hietala et al. 2015, 2017](#); [Runov et al. 2015](#)). We first removed the bins that were at or below the one-count-level from the measurements. We then combined the (cleaned-up) ESA and SST measurements by interpolating in 3D across the energy gap (at 25 keV) between the instruments. The lowest SST energy channels (<35 keV) on P2 were excluded from the interpolation due to degradation effects.

Note that the distribution slices only show the features that are still above the one-count-level after the observed (and cleaned-up) distribution has been interpolated into the slice plane.

D. SENSITIVITIES OF THE ESA AND SST INSTRUMENTS

Figure 5 shows four one-dimensional spectra from ARTEMIS P1 spacecraft obtained at 19:15:04-19:15:08 UT (a) and 20:13:49-20:13:53 UT (b) and from P2 spacecraft at times 19:17:19-19:17:23 UT (c) and 20:13:56-20:14:01 UT (d) on 8 October 2013. The red and blue diamonds show measurements of the ESA and SST instruments, respectively. The red dashed lines and blue dash-dotted lines represent one-count levels of the ESA and SST, respectively. We mark FAB and gyrating ions on panels (a) and (b).

We see that, on average, the sensitivity of the ESA instruments does not permit the detection of the suprathermal ions with energies between 2 keV and 20 keV for the IP shock studied here. Similarly, the SST instrument does not observe ions with energies above 200 keV.

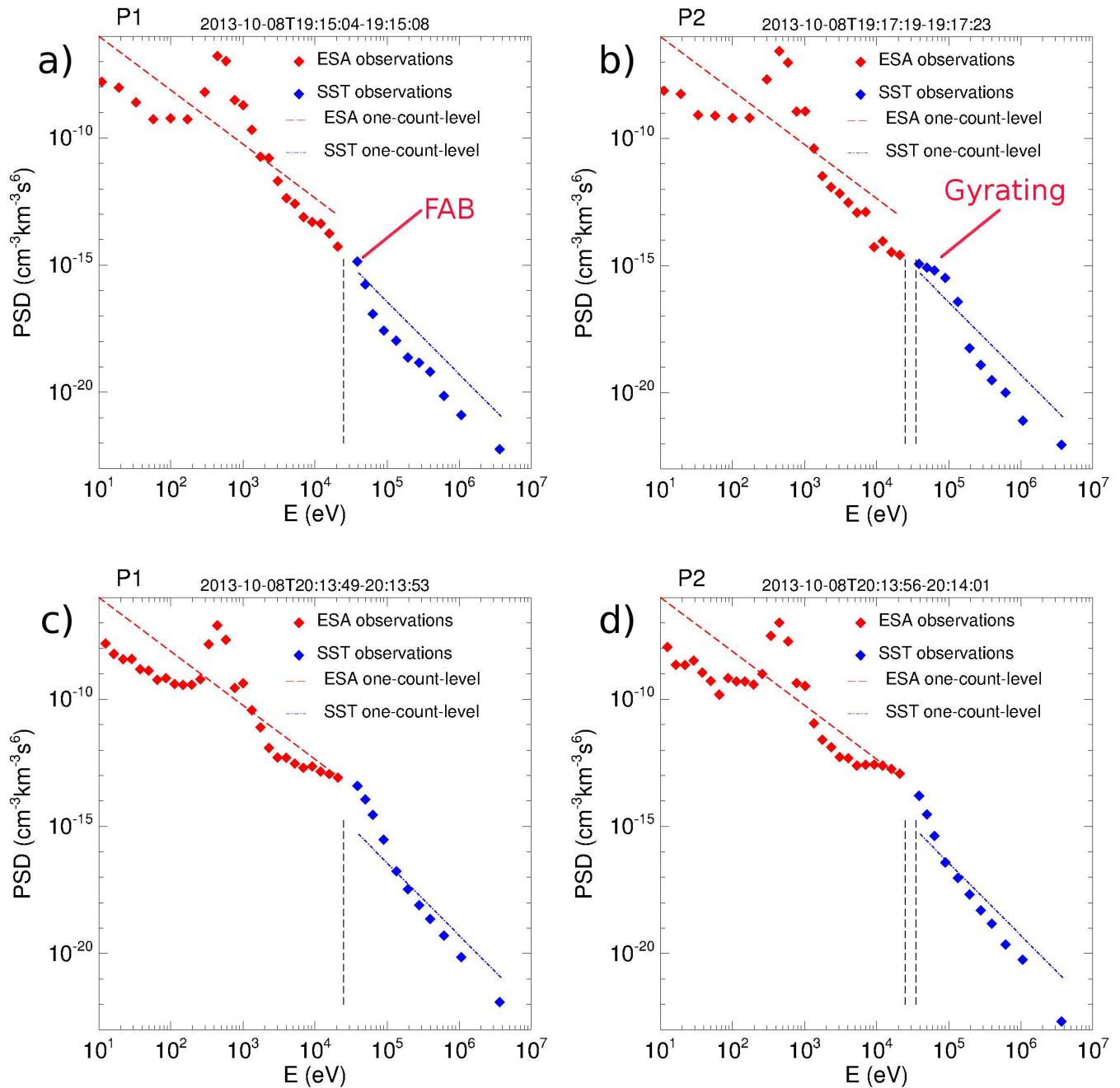


Figure 5. 1D spectra obtained by ARTEMIS P1 spacecraft at 19:15:04-19:15:08 UT (a) and 20:13:49-20:13:53 UT (c) and by P2 spacecraft at 19:17:19-19:17:23 UT (b) and 20:13:56-20:14:01 UT (d) on 8 October 2013. Red and blue diamonds represent ESA and SST data, respectively. The red dashed lines represent the one-count level of the ESA instrument and the blue dash-dotted lines show the one-count level of the SST instrument. Vertical dashed black lines delimit ESA data from SST data. FAB and gyrating ions are marked on panels (a) and (b).